Guerin, G., Rupar, P. A., Molev, G., Manners, I., Hiroshi, J., & Winnik, M. (2016). Lateral Growth of 1D Core-Crystalline Micelles upon Annealing in Solution. *Macromolecules*, *49*(18), 7001-7014. https://doi.org/10.1021/acs.macromol.6b01487

Lateral Growth of 1D Core-Crystalline Micelles upon Annealing in Solution

Gerald Guerin,[1] Paul Rupar,[2] Gregory Molev,[1] Ian Manners,[2] Hiroshi Jinnai*[3], and Mitchell A. Winnik*[1]

1. *Department of Chemistry, University of Toronto, 80 St. George Street, Toronto, ON, M5S 1H6*
2. *School of Chemistry, University of Bristol, Bristol UK, BS8 1TS*
3. *Institute of Multidisciplinary Research for Advanced Materials, Tohoku University, Katahira, Aoba-ku, Sendai, 980-8577, Japan*

**Corresponding authors: hjinnai@tagen.tohoku.ac.jp ; mwinnik@chem.utoronto.ca*

ABSTRACT

The emergence of one-dimensional (1D) micelles obtained from the crystallization driven self-assembly (CDSA) in solution of crystalline-coil block copolymers has opened the door to the fabrication of a variety of sophisticated structures. While the development of these fascinating nanomaterials is blossoming, there is very little fundamental work dedicated to understanding the morphological evolution of these 1D micelles in solution. Here, using a combination of transmission electron microscopy, electron tomography, and static and dynamic light scattering, we studied the effect of annealing on a solution of 1D seed fragments formed by the self-assembly of a crystalline-coil poly(ferrocenyldimethylsilane)-*block*-poly(isoprene) (PFS-*b*-PI) block copolymer. Interestingly, by electron tomography, we observed a slight thinning of the crystalline core as we increased the annealing temperature. We also showed that the packing density of the crystalline block increased, and that the crystalline core of the micelles widened as the seed fragments were annealed at temperatures above 60 °C.

INTRODUCTION

When homopolymers crystallize from solution, they normally fold to form thin plate-like structures (2D crystals) consisting of extended chain crystalline stems with amorphous domains in the fold regions. Kinetic factors play an important role in determining the stem length (i.e., the lamellar thickness) and the fraction of the polymer segments contained within the crystalline domains. Crystal formation is normally not uniform throughout the polymer sample. As a consequence, these semi-crystalline polymer samples exhibit a broad range of melting temperatures, reflecting a distribution of domains with different degrees of crystal perfection. Annealing effects are also important. Upon annealing, the polymer segments can reorganize to improve the packing within the crystal. In this way, the degree of crystallinity of a polymer sample depends upon its thermal history.

Coil-crystalline block copolymers in selective solvents can form colloidal objects with a semi-crystalline core.[1] The earliest examples involved planar structures,[2] but recent attention has turned to block copolymers that form elongated fiber-like structures.[3,4] The first examples of rod-like core-crystalline micelles were reported almost 20 years ago for poly(ferrocenyldimethylsilane) (PFS) diblock copolymers.[5-7] Since that time, particularly after

the discovery of 1D seeded growth and crystallization-driven self-assembly of PFS diblock copolymers in 2007,[8] a much broader range of block copolymers have been reported that form fiber-like micelles with a semicrystalline core.[9] Examples include polymer with PFS,[10-15,21] polyacrylonitrile,[22] polycaprolactone,[23-26] polyethylene,[27-29] poly(3-hexylthiophene) (P3HT),[30,31] poly(3-heptylselenophene),[32] poly(L-lactide)[33-35] and poly(ferrocenyldimethylgermane)9 as the core-forming block. Compared to block copolymers that form 2D platelet crystals, we have a much poorer understanding of how the semicrystalline polymer chains pack in the core of 1D crystalline micelles, and we also know little about how the semicrystalline core rearranges in response to annealing.

Self-seeding experiments have provided some important information about the distribution of crystallinity in 1D core-crystalline micelles. In these experiments, a suspension of the micelles is heated to the point where the sample appears to dissolve, and then upon cooling, micelles of uniform length are formed. As the sample is cooled and becomes supersaturated, the polymer molecules crystallize onto the edges of the surviving crystallites. The first self-seeding experiments were reported for dilute solutions of PFS_{50}-*b*-PI_{1000}, (PI = polyisoprene, the subscripts refer to the block lengths) in decane.[36] Because long micelles tend to fracture when heated in solution,[37] these self-seeding experiments focused on short micelle crystallites ("seeds") with mean lengths less than 100 nm obtained by sonicating a freshly prepared micelle sample. Subsequently, examples have been reported for other PFS diblock copolymers[38,39] and for a P3HT block copolymer.[31] The lengths of these micelles depended sensitively on the temperature at which the solution was heated. These experiments showed that one could use the self-seeding strategy to obtain micelles of uniform length and also to control their length.

The success of these experiments also demonstrate that the core of these micelles consist of domains of differing crystal perfection such that heating the sample in solution led to selective dissolution of the less crystalline material. We have also found that seed crystallite samples annealed at intermediate temperatures exhibited interesting differences from the self-seeding behavior of those obtained from freshly prepared 1D micelles.[38] Subjected to the same concentration and annealing temperature, the annealed seeds gave shorter micelles, still uniform in length. These observations are consistent with an increase in crystal perfection upon aging or annealing, so that a smaller fraction of the seed crystallites dissolve at a given value of T_a.

Previous experiments had been carried out on very dilute copolymer solutions,[38] typically c = 0.02 mg/mL, where annealing ca. 60 nm long micelle seeds (30 min at a series of temperatures up to 70 °C) led to very long micelles upon cooling. For example a sample annealed at 70 °C yielded uniform micelles approximately 2.6 μm long. Here we examine the influence of the same annealing protocol on the structure of PFS_{53}-*b*-PI_{637} micelles at c = 6 mg/mL, still well below the concentration ($c \approx 50$ mg/mL) where nematic ordering of these rigid-rod micelles might occur.[40] The surprising result for the sample at c = 6 mg/mL is that the length of the micelle seeds did not change substantially upon annealing. This unexpected result provided us with an opportunity to examine how the structure of the micelles evolved with annealing, using a combination of techniques that include multiangle static (SLS) [41] and dynamic (DLS) light scattering, transmission electron microscopy (TEM), and electron tomography.

METHODS

Materials

THF (99+ %) and decane (99+ %) were purchased from Aldrich and used without further purification. The PFS_{53}-*b*-PI_{637} block copolymer ($M_{n,GPC}$ = 56,300, Đ = 1.01) was the same sample reported in Ref.14. Disposable 17 × 60 mm glass cells for light scattering were purchased from Fisher Scientific Chemicals.

Preparation of the micelle solutions

We prepared a relatively concentrated mother solution of PFS_{53}-PI_{637} micelles in decane (c = 6.0 mg mL^{-1}) by heating the polymer in decane for 30 mins at 100 °C, and letting the solution cool to room temperature in air. We then sonicated the solution for three 10 mins intervals to obtain short seeds (number average length evaluated by TEM, $L_{n,TEM}$ = 53 nm). One week later, we prepared 5 vials each containing 0.3 mL of this mother solution and heated each of them for 30 mins at a given temperature (namely, 50, 60, 65, 70 and 75 °C). Each solution was then cooled to room temperature before diluting them few days later to c = 0.01 mg mL^{-1}. The solutions were analyzed by static (SLS) and dynamic (DLS) light scattering, transmission electron microscopy (TEM), and electron tomography.

For electron tomography experiments, 5 nm diameter gold nanoparticles (Au NPs) were placed on the supporting membrane of the TEM grid before deposition of the micelle solution.

The sample was left 2 minutes on the grid and then the excess solution was whisked away by touching the side of the grid with a paper filter. Two samples were studied, one annealed at 50 ^{o}C and one annealed at 75 ^{o}C.

Transmission Electron Microscopy

Bright field TEM micrographs were obtained on a Hitachi H-7000 microscope operating at 100 kV. To prepare the TEM samples, a drop of the diluted annealed seed solution (c = 0.01 mg mL^{-1}) was placed onto a carbon coated copper grid at room temperature. Excess fluid was then removed with a clean piece of filter paper. Before every electron microscopy session, the electron beam was aligned to minimize optical artifacts. Images were analyzed using the software package ImageJ, published by the National Institutes of Health. Statistical length analysis was performed on more than 200 micelles that were traced by hand to determine their contour length. The number average micelle lengths ($L_{n,TEM}$) and the weight average micelle lengths ($L_{w,TEM}$) were calculates using eq. 1, where N is the number of micelles examined in each sample, and L_i is the contour length of the i'th micelle.

$$L_{n,TEM} = \frac{\sum_{i=1}^{N} N_i L_i}{\sum_{i=1}^{N} N_i} \qquad L_{w,TEM} = \frac{\sum_{i=1}^{N} N_i L_i^2}{\sum_{i=1}^{N} N_i L_i} \tag{1}$$

Electron Tomography

Electron tomography experiments were performed on an electron microscope operated at 200 kV (JEM-2200FS, JEOL Co., Ltd., Japan) and equipped with a slow scan charge-coupled device camera (Gatan USC4000, Gatan Inc., USA).[42] Projection images were taken from -70^{o} to 70^{o} at an angular interval of 1^{o}. The tilt series of TEM images were reconstructed according to the conventional protocol: they were aligned by the fiducial marker method using the Au NPs as fiducial markers, then 3D images were reconstructed by the filtered back projection algorithm. The limited range of tilt angles samples is expected to result in an artificial elongation of the cross-sectional slices by about 10%.[43,44] Tilt experiments were carried out on 11 micelles each for samples annealed at 50 °C and 75 °C,

Light Scattering Equipments

Static (SLS) and dynamic light scattering (DLS) measurements were performed using a wide angle light scattering photometer from ALV. The light source was a JDS Uniphase He-Ne laser (λ = 632.8 nm, 35 mW) emitting vertically polarized light. The cells were placed into the ALV/DLS/SLS-5000 Compact Goniometer System and sat in a vat of toluene, which matched the index of refraction of the glass cells. The scattered light was detected by a Dual ALV-High Q.E. APD avalanche photodiode module, interfaced to the ALV-5000/EPP multiple tau digital. All measurements were carried out at 20 °C. The angular range consisted of scattering angles between 20º and 150º at 5º intervals for the samples that were annealed at 23, 50, 60, 65 and 70 ºC, and at 2º intervals for the sample annealed at 75 ºC. Toluene was used as the standard in the SLS measurements.

RESULTS AND DISCUSSION

A solution of rod-like PFS_{53}-PI_{637} micelles was prepared by heating a sample of polymer in decane (c = 6.0 mg/mL) to 100 ºC for 30 min, where the polymer dissolves, and then allowing the solution to cool in air to room temperature. These micelles obtained were polydisperse in length with a mean length > 1 μm. This solution was then subjected to mild sonication (23 °C, 3 × 10 min, 60 watt cleaning bath) to obtain a solution of micelle fragments that we will refer to as seeds. A TEM image of the micelle fragments obtained in this way, after aging 3 days at 23 °C, is presented in Figure 1A and the corresponding histogram of micelle lengths is presented in Figure 1B. To obtain these and other histograms, we measured the lengths of more than 200 micelles for each sample using the software ImageJ. From the histogram, one can see that the seed fragments have a broad length distribution characterized by a slightly asymmetric distribution centered at ca. 50 nm with a long tail consisting of micelles > 100 nm long that survived the sonication process. This is the sample (the "mother solution") used for all of the annealing experiments described below.

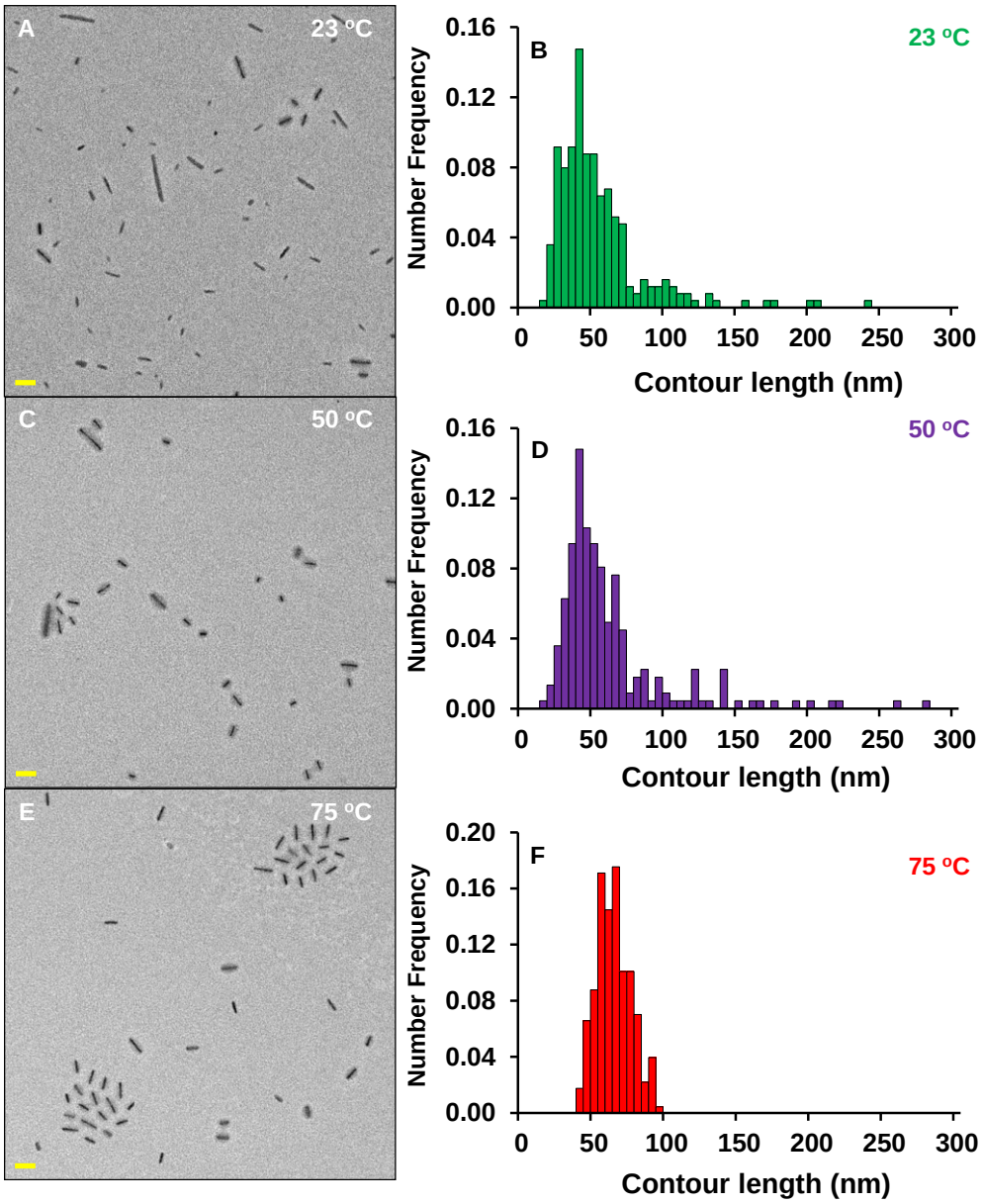

Figure 1: TEM images of PFS_{53}-PI_{637} seeds that were annealed at A) 23 °C, C) 50 °C, and E) 75 °C, and corresponding histograms of the length distribution of PFS_{53}-PI_{637} seeds that were annealed at B) 23 °C, D) 50 °C, and F) 75 °C., as evaluated from the TEM image analysis of more than 200 seeds for each sample For all TEM images the scale bar corresponds to 100 nm.

Aliquots of the mother solutions (0.3 mL) were placed in vials and annealed for 30 min at various temperatures (50, 60, 65, 70 and 75 °C) for 30 min, then allowed to cool to 23 °C and age for 3 days. TEM images and the corresponding histograms for the samples annealed at 50 °C are presented in Figs. 1C and D, and for the samples annealed at 75 °C in Figs. 1E and F.

Corresponding TEM images and histograms of seeds annealed at 60, 65 and 70 ^{o}C are presented in Figure S1, Supporting Information (SI). The histogram for the sample heated at 50 °C is very similar to that of the as prepared micelle seed crystallites. In contrast, more pronounced changes were observed for the sample annealed at 75 °C. The distribution of contour lengths narrowed considerably and the maximum in the distribution shifted from 50 nm to a value closer to 75 nm. No micelles longer than 100 nm could be observed in the TEM images and, in addition, no micelles shorter than 35 nm could be observed. The latter observation suggests that these shorter micelles either dissolved under the annealing conditions or grew longer. We summarize the TEM image analysis of samples obtained from the seed solutions annealed at all of the temperatures both as dot-distribution plots and box-and-whiskers plots shown in Figure 2A.

Figure 2A is particularly useful since it summarizes the most important information that one learns from the contour length histograms obtained from TEM images such as those shown in Figure 1. For example, we see that as the annealing temperature was increased, the maximum length of the seeds that we could find on the TEM grid, L_{max}, decreased, while the minimum length, L_{min}, increased. At low annealing temperatures (23 and 50 ^{o}C), the number average length, $L_{n,TEM}$, is close to the 3rd quartile of the distribution and far from the median length, which indicates that the contour length distribution is asymmetric with a tail to large seed lengths as we see in Figure 1B and 1D. For seed samples annealed at higher temperatures, the 1st and 3rd quartile become closer to each other and the median length is more centered, as one would expect when a distribution becomes narrower and more symmetrical. The value of $L_{n,TEM}$ also becomes equal to the value of the median length.

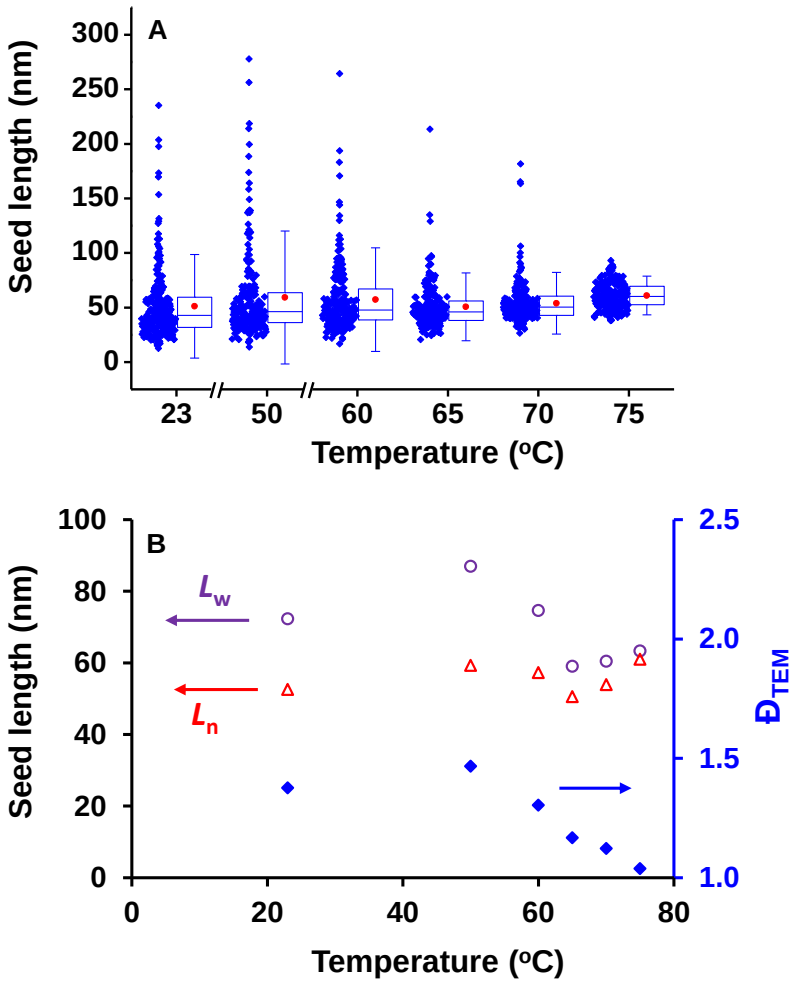

Figure 2: A) Box-and-whiskers plots of the seed length obtained from the TEM image analyzed from seed solution prepared at different annealing temperatures. For each temperature the plot shows the contour length distributions of the PFS_{53}-PI_{637} seeds (blue dots) as well as the median length, the first quartile (only 25% of the seeds are shorter than this value), the third quartile (only 25% of the seeds are longer than this value), the number average length, $L_{n,TEM}$ (red dot), and the standard deviation (horizontal lines). B) Plot of the weight average length evaluated from TEM image analysis, $L_{w,TEM}$, as well as $L_{n,TEM}$ and the dispersity Đ = $L_{w,TEM}/L_{n,TEM}$.

From analysis of the TEM images we also evaluated the weight average length of the seeds, $L_{w,TEM}$, for each annealing temperature. From $L_{w,TEM}$, we calculated the dispersity in lengths, Đ = $L_{w,TEM}/L_{n,TEM}$, for each sample history. Figure 2B shows the evolution of $L_{w,TEM}$, $L_{n,TEM}$, and Đ as a function of T_a. On the one hand, one observes that $L_{n,TEM}$ evolved similarly to $L_{w,TEM}$, since both average lengths decreased with increasing temperature for $T_a \leq 65$ °C, and above this temperature, both $L_{n,TEM}$ and $L_{w,TEM}$ increased with T_a. On the other hand, Đ increased slightly

from T_a = 23 to 50 ºC and then decreased monotonically with T_a from Đ = 1.46 at lower temperatures to Đ = 1.04 at 75 °C. The evolution of Đ as a function of T_a confirms the narrowing of the distribution in seed lengths inferred from Figs 1D,F as the annealing temperature was increased from 50 to 75 ºC.

Light scattering results

The samples described in Figure 2 were then examined by multi-angle SLS and DLS measurements to obtain more detailed characteristics of these micelles in solution. For these measurements, the samples were diluted to c = 0.01 mg/mL to minimize the interactions between the micelles and to ensure that the structure factor would be negligible. All measurements were carried out at room temperature, 23 °C.

Zimm plots and DLS measurements. Analysis of the SLS data in terms of a Zimm plot provides a key insight into the effect of annealing on 1D crystal structure. In Figure 3A we compare plots of Kc/R versus q^2 for the samples annealed at 50 and 75 °C. In this analysis, $K = 4\pi^2 n_D^2 (dn/dc)^2 / (N_A \lambda^4)$ and N_A, λ, dn/dc, and n_D are, respectively, Avogadro's number, the incident wavelength (632.8 nm), the refractive index increment and the refractive index of the solvent; R is the Rayleigh ratio, and q is related to the scattering angle by the expression $q = (4\pi/n\lambda)\sin\theta$. From these plots, we can calculate the weight average molecular weight of each micelle sample M_w and the z-average radius of gyration R_g.

In Figure 3A we see that the slope of the plot of Kc/R vs q^2 is less steep for the sample heated at 75 ºC than that for the sample annealed at 50 ºC, and the value of the ordinate at the origin is lower, indicating that the weight average molecular weight of the seeds annealed at 75 ºC is larger than that of the seeds annealed at 50 ºC ($M_w = 14.3 \times 10^6$ g mol^{-1} at 50 ºC, and $M_w = 16.7 \times 10^6$ g mol^{-1} at 75 ºC). We also found that increasing the annealing temperature from 50 to 75 ºC led to a decrease of R_g (R_g = 39 nm for the sample annealed at 50 ºC, and R_g = 31 nm when the sample was annealed at 75 ºC). We learn that annealing the seed micelles at 75 ºC led to structures that were shorter and heavier than those annealed at 50 ºC, implying that they became denser as the annealing temperature increased.

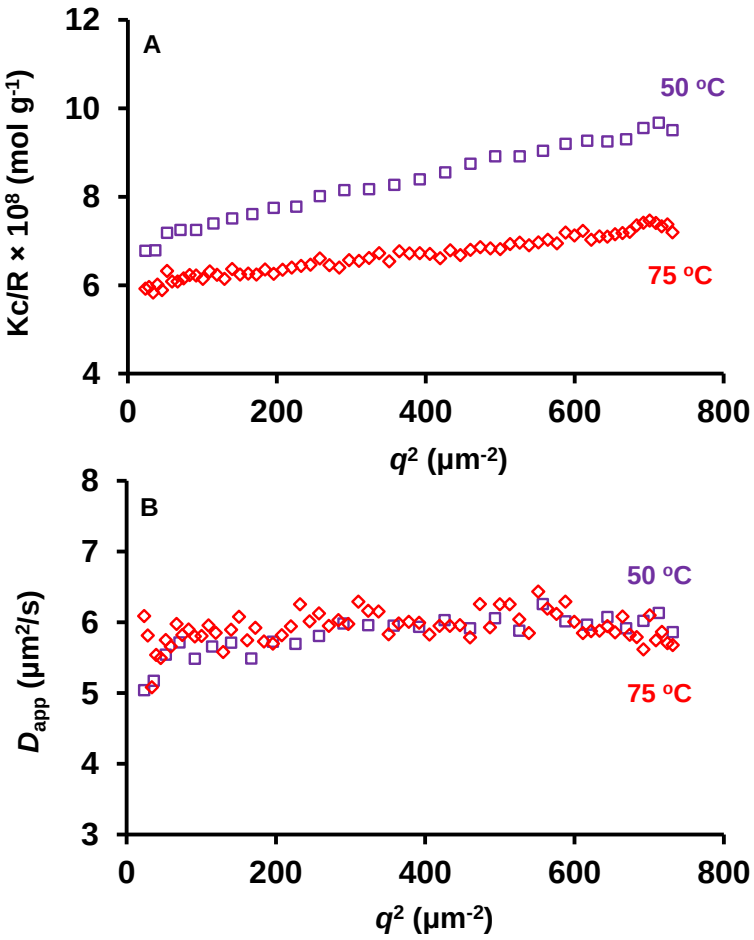

Figure 3: A) Plot of Kc/R versus q^2 for a PFS_{53}-PI_{637} seed solution after they were heated at 50 °C (purple open squares), and at 75 °C (red squares). B) Plot of the diffusion coefficient, $D_{app} = \Gamma/q^2$, versus q^2, where Γ is the decay rate for the same solutions as in A). In Fig. 3A we plotted the trend line for both plots, but for the sample heated at 50 °C, we did not consider the two first points (at low q values). The concentration of the solution for the self-seeding experiments was c = 6.0 mg mL^{-1} and the samples were diluted to a concentration c = 0.01 mg mL^{-1} before performing the SLS and DLS experiments.

For each scattering angle, we also recorded the normalized electric field correlation function, $g^{(1)}(t_c)$ (where t_c is the delay time) of the seed solution. We fitted each correlation function with a cumulant expansion to the second order to extract the decay rate of the correlation function, Γ.[45] After averaging Γ over the three runs, we calculated the apparent diffusion coefficient of the seeds in decane at 23 °C, D_{app}, using the relationship $D_{app} = \Gamma/q^2$. Figure 3B shows the plot of D_{app} as a function of q^2. Zimm plots and plots of D_{app} versus q^2 obtained for seeds solutions that were annealed at T_a = 23, 60, 65 and 70 °C are shown in Figures S2-S6. In each of these

examples, D_{app} is almost constant with q^2, suggesting that the seed micelles behave like spheres. This behavior was to be expected since that the hydrodynamic diameter of the seeds (ca. 80 nm) is close to their length as shown in Table SVV, where we compare these lengths to values of the apparent hydrodynamic radius, $R_{h,app}$, deduced from the Stokes-Einstein relationship.

Form factor analysis of the SLS data. The SLS data for all of the samples, including the as-prepared seed sample at 23 °C, were also fitted using the form factor of a thick rigid rod, $P(q)$:

$$\frac{Kc}{R} = \frac{1}{M_0 \, N_{agg,L} \, P(q)} \tag{2}$$

where M_0 is the weight average molecular weight of a polymer chain, and $N_{agg,L}$ is the weight average linear aggregation number (the mass per unit length expressed as the number of polymer chains per nanometer). $P(q)$ is given by the expression [46]

$$P(q) = \int_0^{\pi/2} \left[2\, j_0\left(\frac{q\, L_{w,SLS} \cos(\beta)}{2} \right) \frac{J_1(q\, R_c \sin(\beta))}{q\, R_c \sin(\beta)} \right]^2 \sin(\beta)\, d\beta \tag{3}$$

where $j_0(x)$ is the zero-order spherical Bessel function of the first kind, while $J_1(x)$ is the first order Bessel function, $L_{w,SLS}$ is the weight average length of the seeds, and R_c is the radius of the seed cross-section.

From values of $L_{w,SLS,}$ R_c and $N_{agg,L}$. we calculated the weight average molecular weight of the seeds, $M_{w,fit} = L_w \times N_{agg,L} \times M_0$, as well as their radius of gyration, $R_{g,fit}$, given by: $R_{g,fit} = [L_w^2/ 12 + R_c^2/2]^{0.5}$. In Table S1 we compare the values of M_w and R_g obtained from the Zimm plots and from the form factor analysis (eq 2) for all the annealing temperatures studied. In this Table, we also added values of M_w and R_g deduced from Guinier plots [ln(Kc/R) versus q^2]. The three different approaches led to very similar values of M_w and R_g at all the annealing temperatures studied, demonstrating internal consistency in the data analysis.

To have a better understanding of the effect of the annealing temperature on the structure of the seed micelle, we examine the T_a dependence of M_w, $L_{w,SLS}$, and $N_{agg,L}$ in Figure 4. The results are also summarized in Table 1. Interestingly, the three plots in Fig. 4 show very distinct trends. In Fig. 4A, one observes that up to 60 °C, M_w decreased from 15.0×10^6 g mol^{-1} at 23 °C to 12.4

$\times 10^6$ g mol^{-1}, then M_w steeply increased to $M_w = 16.8 \times 10^6$ g mol^{-1} at 75 ^oC. At the same time, the weight average length of the seeds, $L_{w,SLS}$, (Fig. 4B) decreased monotonically from 118 nm at 23 ^oC to $L_{w,SLS}$ = 70 nm at 70 ^oC. The seeds then appear to slightly increase in length to reach an average value of $L_{w,SLS}$ = 82 nm at 75 ^oC. Finally Fig 4C shows that $N_{agg,L}$ remained constant (equal to $N_{agg,L} \approx 2.2$ chains nm^{-1}) when the seeds were heated below 60 ^oC, but increased to $N_{agg,L}$ = 3.6 chains nm^{-1} as T_a increased up to 75 ^oC.

Table 1: Values of M_w, R_g, obtained from the Zimm plots and $L_{w,SLS}$, and $N_{agg,L}$ deduced from form factor analysis of the SLS data.

Annealing temperature (^oC)	10^{-6} M_w (g/mol)[a]	R_g (nm)[a]	$L_{w,SLS}$ (nm)[b]	$N_{agg,L}$ (chains/nm)[b]
23	15.0	41	118	2.2
50	14.3	39	116	2.2
60	12.4	35	98	2.2
65	12.6	32	92	2.5
70	13.5	28	70	3.4
75	16.8	31	82	3.6

a. M_w and R_g were obtained from the slope and ordinate at the origin of the Zimm plots

b. $L_{w,SLS}$ and $N_{agg,L}$ were deduced from the form factor analysis of the SLS data.

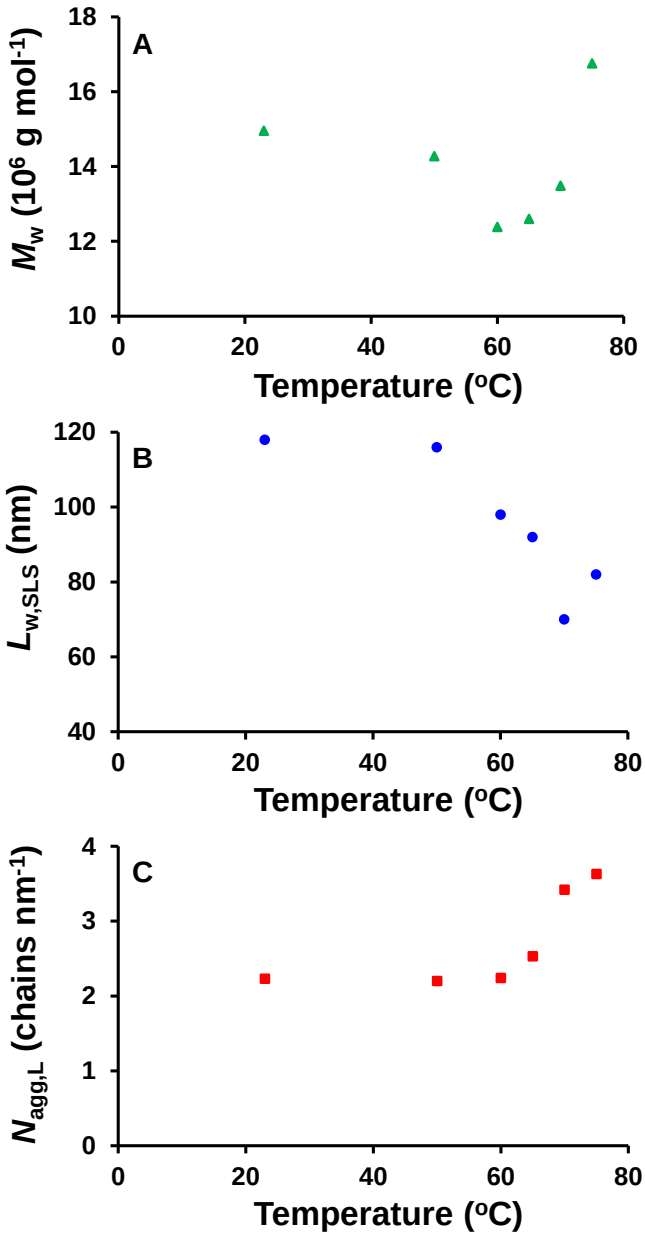

Figure 4. Plots of A) M_w, B) $L_{w,SLS}$, and C) $N_{agg,L}$, as a function of annealing temperature for a PFS_{53}-PI_{637} seed solution of concentration c = 6.0 mg mL^{-1}. M_w was calculated from the Zimm plots, while $L_{w,SLS}$, and $N_{agg,L}$, were obtained from equations 2 and 3, main text.

From these three different plots, one sees that the evolution of the seed micelle structure as a function of annealing temperature can be separated in two main regimes. Up to 60 ºC, $N_{agg,L}$ remained constant, while $L_{w,SLS}$ decreased, leading to a decrease in the weight average molecular weight of the seed micelles. We have previously shown that micelles of PFS_{50}-*b*-PI_{1000} in decane, heated at temperatures between 40 and 60 °C, were susceptible to fragmentation[37] that increased

significantly for longer micelles. The extent of fragmentation also increased with temperature, but above 60 °C was accompanied by polymer dissolution. The dissolved polymer re-grew onto the ends of the surviving micelles as the solution was cooled back to room temperature. Thus we hypothesize that in this temperature range, the longest of the PFS_{53}-*b*-PI_{637} micelle seeds undergo fragmentation, leading to an increase of the total number of seeds. This assumption is supported by the fact that $N_{agg,L}$ remained constant, and also by the evolution of the length distributions of the seeds obtained by TEM image analysis and presented in Figs. 1 and 2. Above 60 °C, $N_{agg,L}$ increased while $L_{w,SLS}$ decreased. The weight average molecular weight of the seeds however increased over the same temperature range. The increase in $N_{agg,L}$ is an indication of the densification of the seeds, Densification can occur by thickening of the seeds or by improvement of the crystal packing. In both cases, this increase suggests that the semi-crystalline core is sufficiently mobile to reorganize. The densification (or the thickening) of the seed core would be accompanied by a shortening of the seeds, as observed in Fig. 4B. Interestingly, the fact that M_w also increases with T_a when the seeds are annealed above 60 °C indicates that the number of chains per seed increases. Since no unimer was added to the solution, we conclude that some of the seeds dissolved above 60 °C, and that the resulting unimer re-grew on the surviving seeds, increasing their weight average molecular weight.

In previous studies focused on longer micelles, we have shown that there is a good agreement between weight averaged micelle lengths obtained by static light scattering for PFS micelles in solution and the corresponding values determined by TEM analysis on these same samples on a grid. This is an important observation, as it demonstrates that depositing the micelles on a TEM grid does not change their size and shape. In the present study we found that values of $L_{w,SLS}$ were always somewhat larger than those of $L_{w,TEM}$ (Fig. S7A). We attribute this difference to the contribution of the corona chains to the magnitude of $L_{w,SLS}$, as depicted in Fig. S7B. In unstained TEM images, one sees primarily the electron rich core of the seeds, leading to a somewhat smaller value of $L_{w,TEM}$. For longer micelles, the fractional contribution of the corona chains to the micelle length is negligible.

Electron tomography

To obtain further information on the origin of the increase in linear aggregation number of the seed micelles after annealing above 60 °C, we used electron tomography to examine the cross

sections of the micelles. These were challenging measurements, covering tilt angles of -70° to +70°, and only 11 micelles were imaged for each sample. In the absence of measurements at higher tilt angles, we anticipate an artificial elongation of the cross-sectional slices by about 10%.**Error! Bookmark not defined.** With these reservations in mind, we compare results on the micelles annealed 30 min at 50 °C with the sample annealed 30 min at 75 °C. Figure 5 shows representative tomography images of these samples after reconstruction of the 3D images (other images are presented in Figs. S8 and S9). The reconstructed 3D images are shown in orthogonal plots, where the XY slice image is the "top view" and "YZ" and "XZ" slice images are two cross-sectional views. From the XY slice image of the micelles, one observes that the growth front of the seeds is not flat, but tapered, independent of the annealing temperature. Comparison of the XY image with the YZ slice of both micelles shows that the micelles are wider than they are thick, suggesting an overall thin lamellar core shape. The XY slice images, however, do not show substantial differences between the seed micelle annealed at 50 ^{o}C and the micelle annealed at 75 ^{o}C.

The effect of annealing temperature on the seed fragments can better be seen in their slice images in the YZ and XZ planes (Figure 5). YZ plane images of the seed fragments suggest that the thickness of the core of the seed micelles annealed at 50 ^{o}C and at 75 ^{o}C are similar (ca. 6 nm). The XZ slices, however, show that the sample annealed at 50 ^{o}C has a more rounded cross-section, while, the cross section of the micelle seed annealed at 75 ^{o}C looks more like a tilted thin ribbon. Analysis of the XY slice images indicates that the micelle core becomes wider upon annealing at 75 °C. We calculated a number average width $width_{\mathrm{core}}$ = 19 nm for the seed fragments annealed at 50 ^{o}C, while the corresponding mean width of the seed micelles annealed at 75 ^{o}C was 25 nm. The results of the data analysis are summarized in Table S2. They indicate a widening of the PFS core accompanied by a slight thinning upon annealing at 75 ^{o}C.

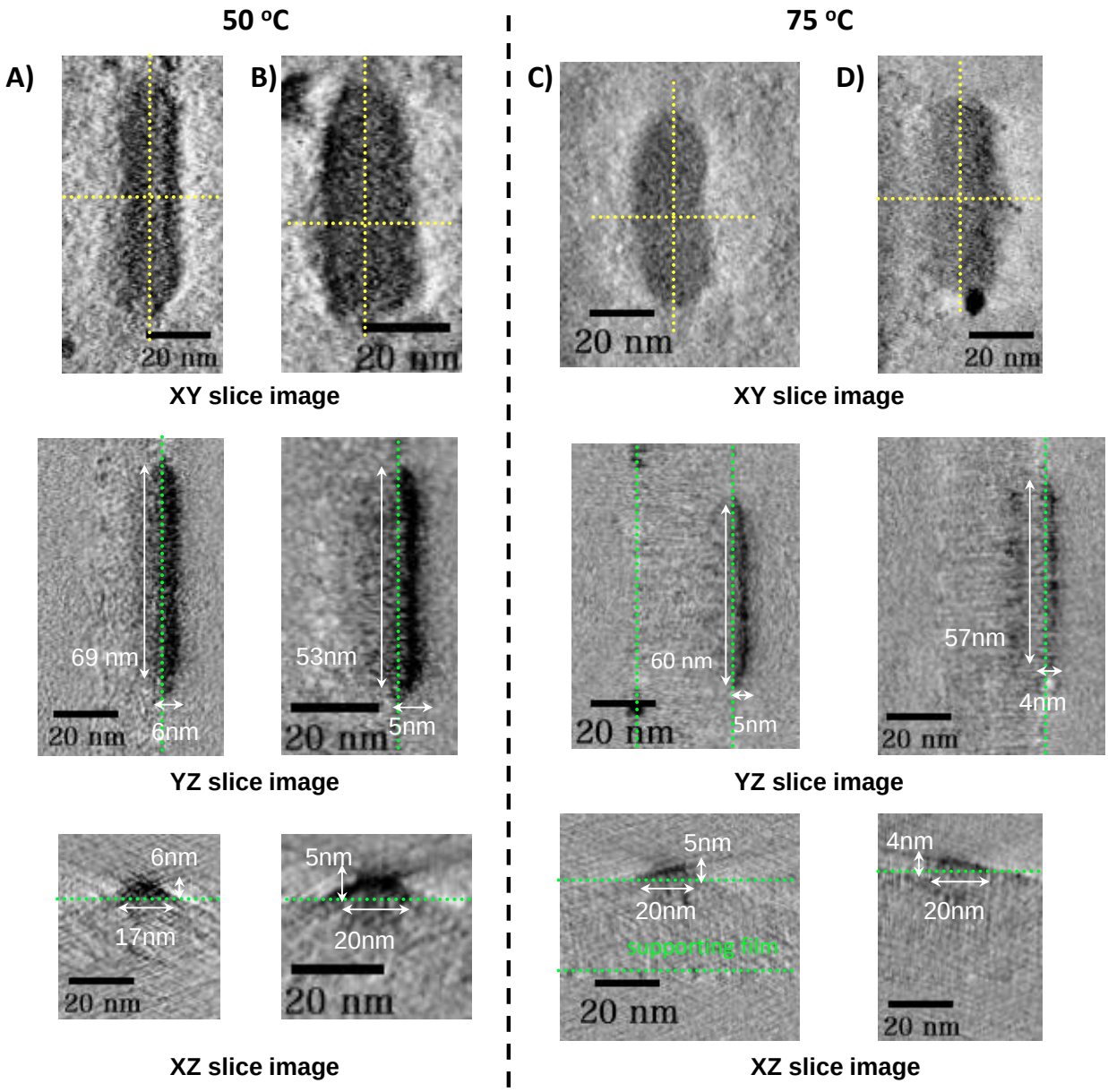

Figure 5: Electron tomography images of PFS_{53}-PI_{637} seeds annealed for 30 minutes at A) and B) 50 °C, and C) and D) 75 °C. For each annealing temperature three orthogonal cross-sectional views are shown from the XY, YZ and XZ planes.

The combination of the results obtained from TEM image analysis, light scattering and electron tomography, offers important insights about the effects of annealing on the reorganization of the crystalline core of the micelles. To have a better understanding of these effects, we need to recall how they were prepared. First a suspension of PFS_{53}-PI_{637} in decane (c = 6.0 mg/mL) was heated to 100 °C for 30 mins to dissolve the polymer and obtain a hot solution of unimer. Then the solution was allowed to cool in air. It quickly became turbid, pointing to

rapid nucleation and growth of the micelles. The solution was then left to age a few days at 23 °C to ensure that the micelles were fully grown (no free unimer remaining in the solution). Finally seed fragments were obtained by mild sonication of the micelle solution. Since mild sonication does not affect the linear aggregation number of the micelles,[47] we infer that the seeds fragments obtained in this way had a crystallinity similar to that of the micelles prior to sonication.

According to Sanchez and DiMarzio,[48] the rapid growth of a polymeric crystal increases the probability of trapping amorphous segments of the polymer at the fold surface. They refer to the amorphous polymer chains trapped at the fold surface of a lamellar crystal as "cilia". From this perspective, we anticipate the presence of significant amounts of PFS trapped as amorphous material outside the crystalline core of the micelles. Several years ago, we reported SAXS measurements on oriented concentrated (75 mg/mL) solutions of very similar of PFS-*b*-PI block copolymer micelles.[49] The main conclusion was that the crystalline domains within the core were highly ordered on a sample annealed at 60 °C for 48 h. In addition the PFS core appeared to contain additional amorphous material.

Our sample (at 6 mg/mL) showed essentially no changes by SLS and TEM following 30 min annealing at 50 °C (cf. Fig. S2). We infer from these results that the crystallinity of this mildly annealed sample is similar to that of the as-prepared seed fragments, and we begin our discussion of the electron tomography results from the perspective that the sample annealed at 50 °C contains a significant amount of amorphous PFS. The amorphous phase is less dense than the ordered crystalline phase.

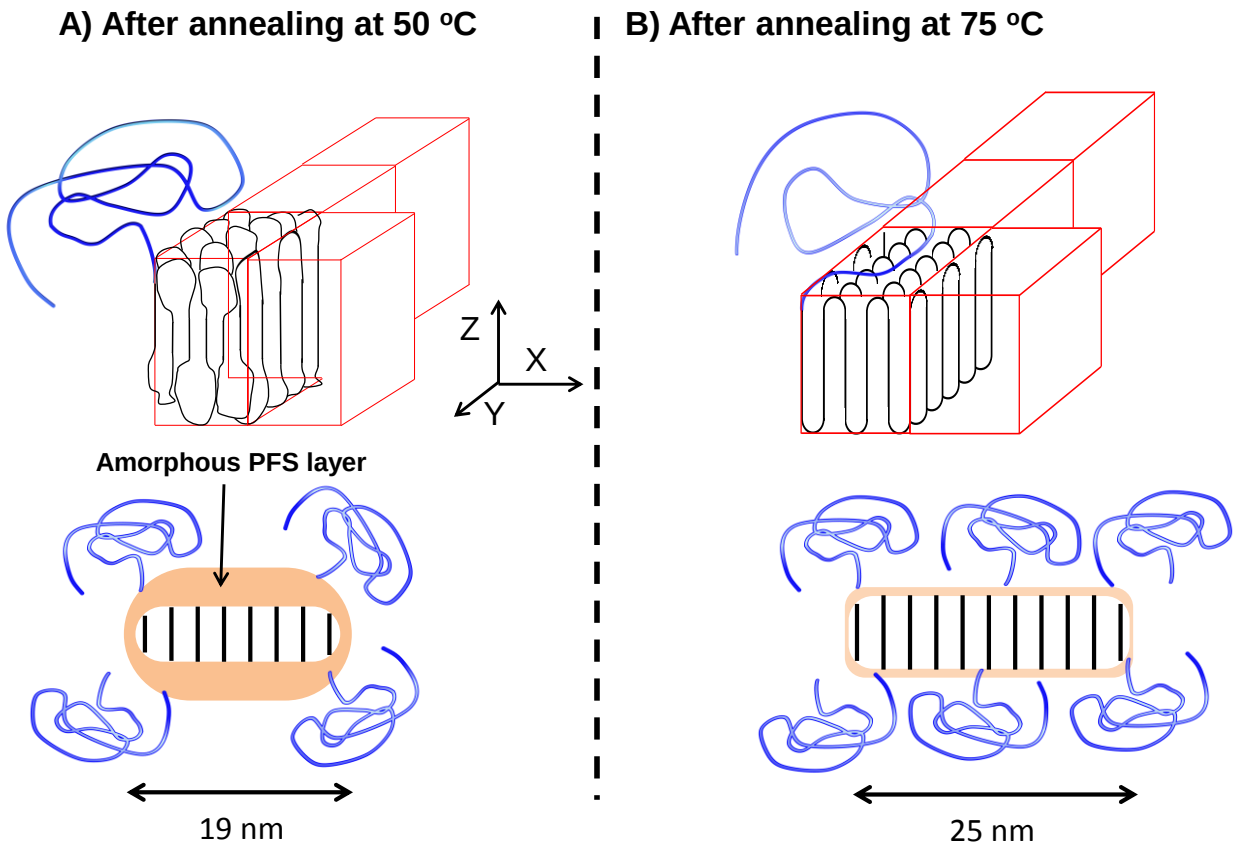

Figure 6. Schematic representation of the seed fragments after being annealed for 30 mins at A) 50 ºC, and B) 75 ºC. Note that crystal growth occurs in the Y-direction. The view of the micelles in the XZ plane is shown in the lower part of the Figure. Annealing the seed fragments at 75 ºC increases the crystallinity of the seed core, favoring a better packing of the PFS segments and decreasing the volume of the amorphous region inside the core. The increased width of the core (*width*$_{core}$) seen by electron tomography accompanied by an increase in $N_{agg,L}$ suggests that annealing the seeds at higher temperatures facilitates addition of PFS$_{53}$-*b*-PI$_{635}$ unimer chains to the lateral edges of the micelles (along the X-axis).

In the electron tomography images of this sample, we detect curvature of the core (Fig. 5A,B, XZ slice image), suggestive of an elliptical shape and partially resembling the cross-section of the amorphous core of a worm-like micelle. After annealing at 75 °C, the core became wider and more rectangular (Fig. 5C,D, XZ slice image). Even more striking, the magnitude of $N_{agg,L}$ increased from 2.2 chains/nm at 50 ºC to 3.6 chains/nm. This increase is too large to be explained only in terms of an increase in core density accompanying an increasing degree of

crystallinity of the PFS in the micelle core. A more reasonable explanation for the increase in $N_{agg,L}$ is that upon cooling after annealing at 75 °C, unimer chains deposit along the sides of the micelle, increasing its width.

Figure 6 depicts various structural features of the micelle before and after annealing at 75 °C. PFS_{50} homopolymer forms elongated rectangular crystals, indicating that crystal growth is asymmetric. The Y-axis in Figure 6 represents the favored growth direction of the PFS core. For a highly crystalline core, one expects the core cross section to be rectangular, and for the long corona chains to limit the lateral growth of the micelles.[50-52] As depicted in Figure 6A, amorphous material on the upper and lower surfaces of the core could impart curvature to the shape of the cross section. Amorphous material at the long edges of the core may also poison lateral growth[53] in the X-direction during micelle formation and limit the width of the micelles. Upon annealing at higher temperatures, the crystallinity of the core increases, "healing" and sharpening the interface between the seed core and the solvent. At these high temperatures (T > 60 °C), some of the seed fragments dissolve, and upon cooling, this unimer adds onto the surviving seeds. This process leads to an increase in M_w as observed by SLS. Moreover, the pronounced increase in $N_{agg,L}$ and the widening of the core seen by electron tomography point to unimer deposition onto the sharp lateral edges of the micelle core formed upon annealing. This lateral growth is depicted in Figure 6B.

Surface density of corona chains and chain folding in the core

To gain deeper insights into the core structure, we consider the effect of annealing on the density of corona chains (σ) attached to the basal surfaces of the semicrystalline core. The value of σ can be evaluated as the ratio of $N_{agg/L}$ (determined by SLS) to the width of the micelle core (determined by electron tomography), $width_{core}$.

$$\sigma = \frac{N_{agg,L}}{width_{core}} \tag{4}$$

For the sample annealed at 50 °C, we found a value of σ_{50} = 0.12 chains/nm^2, which increased slightly to σ_{75} = 0.15 chains/nm^2 after the solution of micelle fragments was annealed at 75 °C.

These low σ values, corresponding to a surface area of 6.9 to 8.6 nm^2/PI chain, suggest that the anchor points of the corona chains are separated by multiple folds of the PFS chains in the core.

A second way to evaluate σ is to acknowledge that PFS micelle fragments are similar to two-dimensional polymer single crystals grown from block copolymers, where the crystalline lamellae is sandwiched between two amorphous layers. [54,55] The surface density of the chains tethered to the crystal surface is related to the crystalline core thickness, d_{cryst}, the density of the core polymer ρ_{cryst} and the molecular weight of the crystalline block M_n^{cryst}, through the expression

$$\sigma = \frac{N_{Av}\,\rho_{cryst}\,d_{cryst}}{2\,M_n^{cryst}} \tag{5}$$

where N_{Av}, is the Avogadro number. The factor of 2 takes account of the fact that the corona chains are attached to both the upper and lower surfaces of the crystalline core. The thickness of the crystalline core can be deduced from the overall thickness of the sandwich, $d_{overall}$:

$$d_{cryst} = d_{overall}\,\upsilon_{cryst} \tag{6a}$$

The volume fraction of the micelle crystalline core, υ_{cryst}, is defined as:

$$\upsilon_{cryst} = \frac{M_n^{cryst}/\rho_{cryst}}{M_n^{cryst}/\rho_{cryst} + M_n^{am}/\rho_{amorph}} \tag{6b}$$

with M_n^{amorph} being the molecular weight of the polymer composing the amorphous layers of the sandwich, and M_n^{cryst} is the molecular weight of the core-crystalline polymer.

In the present system, the PFS core can be reasonably depicted as a layer of crystalline PFS, sandwiched between two layers of amorphous PFS, as drawn in Figure 6. The amorphous part of the PFS core is due to defects in the chain folding during the crystal growth, which means that individual PFS chains occupy portions of both the crystalline and the amorphous regions of the core. We can thus write M_n^{cryst} and M_n^{amorph} as a function of M_n^{PFS}, and of the fractional crystallinity of PFS in the core, w_{crys}:

$$M_n^{cryst} = w_{crys} M_n^{PFS} \tag{7a}$$

$$M_n^{amorph} = \left(1 - w_{crys}\right) M_n^{PFS} \tag{7b}$$

Eqs 7a and 7b combined with eq 6b lead to:

$$\upsilon_{cryst} = \frac{1}{1 + \frac{\left(1 - w_{crys}\right)}{w_{crys}} \frac{\rho_{cryst}}{\rho_{amorph}}} = \frac{\rho_{amorph} w_{crys}}{\rho_{amorph} w_{crys} + \left(1 - w_{crys}\right) \rho_{cryst}} \tag{8}$$

Since only the electron rich PFS block can be observed by electron microscopy, the overall thickness measured by electron tomography corresponds to the thickness of the PFS core. From eq 8, one can express the magnitude of σ in terms of the thickness of the PFS core, d_{core}, and the degree of crystallinity w_{cryst} of the PFS core.

$$\sigma = \frac{N_{Av} \rho_{cryst} d_{core}}{2 M_n^{PFS}} \frac{\rho_{amorph}}{\rho_{amorph} w_{crys} + \left(1 - w_{crys}\right) \rho_{cryst}} \tag{9}$$

Here ρ_{cryst}, the density of crystalline PFS is equal to 1.455 g/cm^3, [56] while the density of amorphous PFS, ρ_{amorph}, is equal to 1.26 g/cm^3. [57]

Using eq 9, we plotted σ as a function of the PFS fractional crystallinity by setting d_{core} = 5.5 nm for the seed fragment solution annealed at 50 ^{o}C (Fig 7A) and d_{core} = 4.5 nm for the seed fragment solution annealed at 75 ^{o}C (Fig 7B). The values of the core thickness measured by electron tomography were corrected to account for the artificial elongation of the core thickness by ca. 10%. This artificial elongation is caused by the tilt range used to image the seed fragments.

Figure 7A shows that for the seed fragment solution annealed at 50^{o}C, σ increases from 0.16 to 0.18 PI chains/nm^2 as w_{cryst} increases from 0 to 1. In this plot, one observes that these calculated values of σ are larger than the experimental value σ_{50} obtained from $N_{agg,L}$ and the core width measured by electron tomography, implying that the core thickness determined by electron tomography leads to an overestimation of the number of PI chains/nm^2. In contrast, when the sample was annealed at 75 ^{o}C, the plot of σ versus fractional crystallinity crosses the value of σ_{75} at a degree of PFS crystallinity of 0.62.

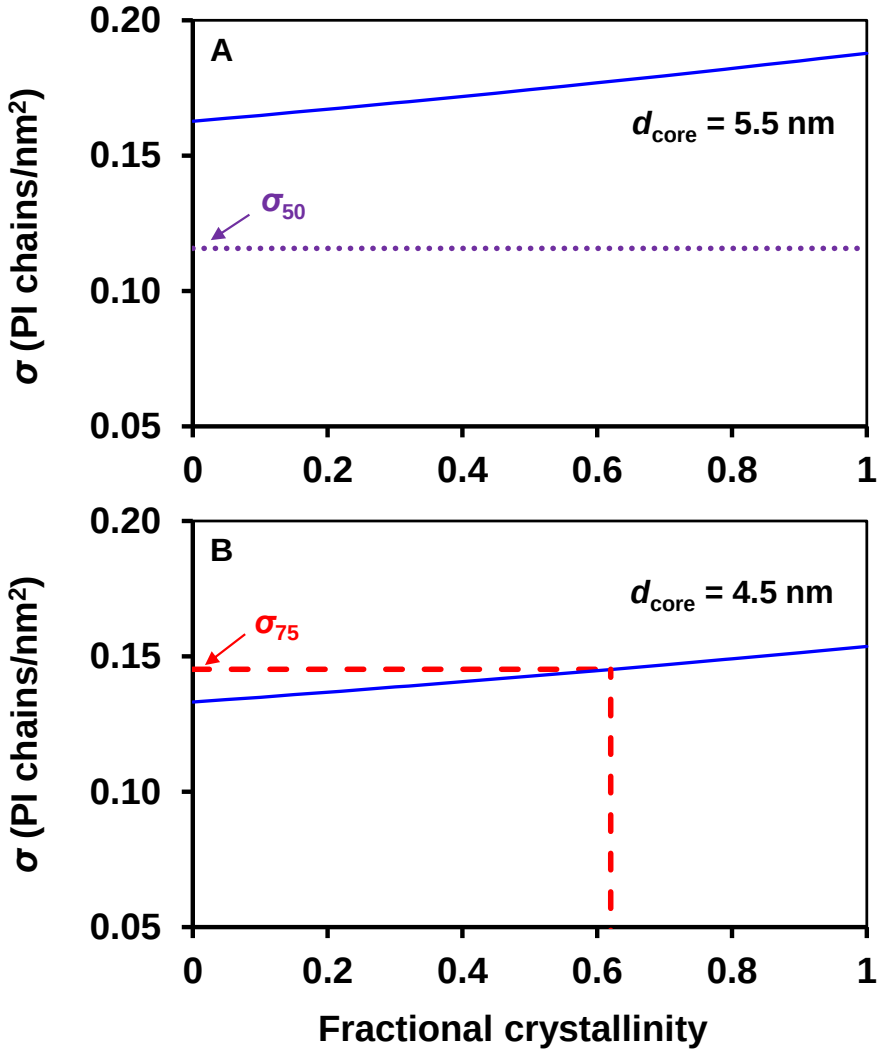

Figure 7. Plot of the calculated surface density of the corona chains (eq. 9), σ as a function PFS crystallinity in the core, for the samples annealed 30 mins at A) 50 °C, and B) 75 °C. These calculations are based on a rectangular cross section model in which the PFS micelle core is treated as a lamellar crystal of thickness d_{cryst} sandwiched between two amorphous PFS domains. Values of σ were calculated considering an overall thickness of the core, d_{core} of (A) 5.5 nm and (B) 4.5 nm, as measured by electron tomography. The horizontal lines represent the values of σ (σ_{50} and σ_{75}) obtained from the ratio of $N_{agg/L}$ to the core width $width_{core}$. From σ_{75}, one can estimate the fraction of crystalline PFS for the sample annealed at 75 °C (w_{cryst} = 0.62).

To have a better understanding of the factors that may affect the values of σ evaluated with eq 9 for the seed fragment annealed at 50 ^{o}C, we first need to recall some key characteristics of this sample. The length distribution of these fragments was rather broad (Đ = 1.46, cf Fig 1D), and the distribution of core thickness for this sample may also be broad. Moreover, the shape of their core cross-section is not perfectly rectangular, but slightly rounded. Because the shape of the core cross-section of the seeds annealed at 50 ^{o}C is not rectangular, the use of eq 9 to evaluate σ may not be correct. These factors help us to understand why the values of σ evaluated with eq 9 do not agree with the value calculated from the ratio of $N_{agg,L}/width_{core}$.

The seed fragments annealed at 75 ^{o}C are narrowly distributed in length (Đ = 1.04, cf Fig 1F), and their core cross-section appears to be rectangular. Here there is good agreement between the values of σ obtained by the two approaches, and gives us confidence in the value of d_{core} = 4.5 nm determined for this sample. We can use this value to gain more information about the PFS in the core of the micelle fragments annealed at 75 °C. With eq 6a, we can evaluate the average thickness of the crystalline lamellar core, obtaining a value d_{cryst} ≈2.6 nm. From the overall core thickness, we can also calculate the number of folds per PFS block. Taking the value of 0.7 nm as the distance between iron atoms in adjacent repeat units of PFS, [56,58] we estimate a fully extended length of ca. 37 nm for the PFS chain in PFS_{53}-*b*-PI_{637}. In terms of this very simple model, a core thickness of 4.5 nm implies ca. 8 folds per PFS chain. By approximating the surface occupied by one fold, S_f, by $S_f = 0.7^2 = 0.49$ nm^2, we can also calculate the surface occupied by one PFS block, $S_{PFS} = 0.49 \times 8 = 3.9$ nm^2. Since half of the corona chains protrude from each side of the lamella, the surface occupied by one PI block should be given by $S_{PI} = 2 \times S_{PFS} = 7.8$ nm^2, in reasonable agreement with the value of 6.9 nm^2 obtained from eq. 4.

In summary, we have studied the self-seeding behavior of a solution of PFS_{53}-*b*-PI_{637} micelle fragments at c = 6.0 mg/mL at different temperatures. The first intriguing observation was that, unlike much lower concentrations, the length of the seed fragments did not increase noticeably with annealing temperature, suggesting that at 6 mg/mL a much smaller fraction of the polymer dissolved upon heating than similar micelle fragments at c = 0.02 mg/mL. For example, at c = 0.02 mg/mL, short seed fragments of PFS_{53}-*b*-PI_{637} ($L_{n,TEM}$ = 63 nm) annealed a 70 ^{o}C for 30 mins grew to ca. 2.6 μm after cooling to 23 °C, while under the same annealing conditions, micelle fragments of PFS_{53}-*b*-PI_{637}, similar in starting length ($L_{n,TEM}$ = 53 nm), at 6.0 mg/mL

showed no increase in length ($L_{n,TEM}$ = 54 nm). We also found a narrowed length distribution for the more concentrated sample after annealing at 70 or 75 °C.

It has been shown previously for bulk samples of PFS homopolymer that the degree of crystallinity increases upon annealing for various times at 90 °C.[59] This result is consistent with the evolution of the morphology of the PFS_{53}-*b*-PI_{637} micelle core examined here. One of the most important conclusions of our study is that annealing of these micelle fragments at temperatures above 60 °C leads to an increase in width as a consequence of deposition of unimer along the lateral edges of the micelle cores.

These observations of the evolution of core morphology may offer ways to fabricate more robust or more sophisticated structures by crystallization-driven self-assembly. The effect of seed concentration upon dissolution at different temperatures and the impact of high annealing temperatures on the morphology of the seed core are under investigation and will be the topics of future publications.

SUPPORTING INFORMATION

The supporting information is available free of charge via the Internet at http://pubs.acs.org.

The supporting Information contains: tables summarizing the data obtained by static light scattering (Table S1) and the data obtained by electron tomography image analysis (Table S2). Static and dynamic light scattering plots of the samples annealed at 23, 50, 60, 70 and 75 ^{o}C (Figures S1 – S6), Plot of the weight average length of the seeds as a function of annealing temperature as determined by SLS and by TEM image analysis (Figure S7). Electron tomography images of the samples annealed at 50 and 75 ^{o}C (Figures S8-S9).

ACKNOWLEDGMENTS

We thank T. Toriyama for carrying out the Electron Tomography imaging measurements. The Toronto authors thank NSERC Canada for their support. I.M. thanks the EU and EPSRC for support.

REFERENCES

[1] Crassous, J. J.; Schurtenberger, P.; Ballauff, M.; Mihut, A. M. Design of Block Copolymer Micelles via Crystallization. *Polymer* **2015**, *62*, A1–A13

[2] Lotz, D. B.; Kovacs, P. D. A. J.; Bassett, D. G. A.; Keller, P. D. A. Properties of Copolymers Composed of One Poly-Ethylene-Oxide and One Polystyrene Block. *Kolloid-Z.u.Z.Polymere* **1966**, *209* (2), 115–128.

[3] Qian, J.; Zhang, M.; Manners, I.; Winnik, M. A. Nanofiber Micelles from the Self-Assembly of Block Copolymers. *Trends Biotechnol.* **2010**, *28* (2), 84–92.

[4] Schmelz, J.; Schacher, F. H.; Schmalz, H. Cylindrical Crystalline-Core Micelles: Pushing the Limits of Solution Self-Assembly. *Soft Matter* **2013**, *9* (7), 2101.

[5] Massey, J.; Power, K. N.; Manners, I.; Winnik, M. A. Self-Assembly of a Novel Organometallic−Inorganic Block Copolymer in Solution and the Solid State: Nonintrusive Observation of Novel Wormlike Poly(ferrocenyldimethylsilane)-B-Poly(dimethylsiloxane) Micelles. *J. Am. Chem. Soc.* **1998**, *120*, 9533–9540.

[6] J. A. Massey, K. Temple, L. Cao, Y. Rharbi, J. Raez, M. A. Winnik, I. Manners, Self-Assembly of Organometallic Block Copolymers: The Role of Crystallinity of the Core-Forming Polyferrocene Block in the Micellar Morphologies formed by Poly(ferrocenylsilane-*b*-dimethylsiloxane) in *n*-Alkane Solvents, *J. Am. Chem. Soc.*, 122, 11577-11584 (2000)

[7] Cao, L.; Manners, I.; Winnik, M. A. Influence of the Interplay of Crystallization and Chain Stretching on Micellar Morphologies: Solution Self-Assembly of Coil−Crystalline Poly(isoprene-Block-Ferrocenylsilane). *Macromolecules* **2002**, *35*, 8258–8260.

[8] Wang, X.; Guerin, G.; Wang, H.; Wang, Y.; Manners, I.; Winnik, M. A. Cylindrical Block Copolymer Micelles and Co-Micelles of Controlled Length and Architecture. *Science* **2007**, *317* (5838), 644–647.

[9] Gadt, T.; Ieong, N.; Cambridge, G.; Winnik, M.; Manners, I. Complex and Hierarchical Micelle Architectures from Diblock Copolymers Using Living, Crystallization-Driven Polymerizations. *Nat. Mater.* **2009**, *8*, 144–150.

[10] Qi, F.; Guerin, G.; Cambridge, G.; Xu, W.; Manners, I.; Winnik, M. A. Influence of Solvent Polarity on the Self-Assembly of the Crystalline–Coil Diblock Copolymer Polyferrocenylsilane-B-Polyisoprene. *Macromolecules* **2011**, *44* (15), 6136–6144.

[11] Rupar, P. A.; Chabanne, L.; Winnik, M. A.; Manners, I. Non-Centrosymmetric Cylindrical Micelles by Unidirectional Growth. *Science* **2012**, *337* (6094), 559–562.

[12] Nazemi, A.; Boott, C. E.; Lunn, D. J.; Gwyther, J.; Hayward, D. W.; Richardson, R. M.; Winnik, M. A.; Manners, I. Monodisperse Cylindrical Micelles and Block Comicelles of Controlled Length in Aqueous Media. *J. Am. Chem. Soc.* **2016**, *138* (13), 4484–4493.

[13] Guerin, G.; Cambridge, G.; Soleimani, M.; Mastour Tehrani, S.; Manners, I.; Winnik, M. A. Form Factor of Asymmetric Elongated Micelles: Playing with Russian Dolls Has Never Been so Informative. *J. Phys. Chem. B* **2014**, *118* (36), 10740–10749.

[14] Rupar, P. A.; Cambridge, G.; Winnik, M. A.; Manners, I. Reversible Cross-Linking of Polyisoprene Coronas in Micelles, Block Comicelles, and Hierarchical Micelle Architectures Using Pt(0)–Olefin Coordination. *J. Am. Chem. Soc.* **2011**, *133* (42), 16947–16957.

[15] Li, X.; Gao, Y.; Boott, C. E.; Winnik, M. A.; Manners, I. Non-Covalent Synthesis of Supermicelles with Complex Architectures Using Spatially Confined Hydrogen-Bonding Interactions. *Nat Commun* **2015**, *6*, 8127.

[16] Qiu, H.; Hudson, Z. M.; Winnik, M. A.; Manners, I. Multidimensional Hierarchical Self-Assembly of Amphiphilic Cylindrical Block Comicelles. *Science* **2015**, *347* (6228), 1329–1332.

[17] Jia, L.; Zhao, G.; Shi, W.; Coombs, N.; Gourevich, I.; Walker, G. C.; Guerin, G.; Manners, I.; Winnik, M. A. A Design Strategy for the Hierarchical Fabrication of Colloidal Hybrid Mesostructures. *Nat Commun* **2014**, *5*.

[18] He, F.; Gädt, T.; Manners, I.; Winnik, M. A. Fluorescent "Barcode" Multiblock Co-Micelles via the Living Self-Assembly of Di- and Triblock Copolymers with a Crystalline Core-Forming Metalloblock. *J. Am. Chem. Soc.* **2011**, *133*, 9095–9103.

[19] Hudson, Z. M.; Lunn, D. J.; Winnik, M. A.; Manners, I. Colour-Tunable Fluorescent Multiblock Micelles. *Nat Commun* **2014**, *5*.

[20] Zhou, H.; Lu, Y.; Qiu, H.; Guerin, G.; Manners, I.; Winnik, M. A. Photocleavage of the Corona Chains of Rigid-Rod Block Copolymer Micelles. *Macromolecules* **2015**, *48* (7), 2254–2262.

[21] Gao, Y.; Qiu, H.; Zhou, H.; Li, X.; Harniman, R.; Winnik, M. A.; Manners, I. Crystallization-Driven Solution Self-Assembly of Block Copolymers with a Photocleavable Junction. *J. Am. Chem. Soc.* **2015**, *137* (6), 2203–2206.

[22] Lazzari, M.; Scalarone, D.; Vazquez-Vazquez, C.; Lòpez-Quintela, M. A. Cylindrical Micelles from the Self-Assembly of Polyacrylonitrile-Based Diblock Copolymers in Nonpolar Selective Solvents. *Macromol. Rapid Commun.* **2008**, *29* (4), 352–357.

[23] He, W.-N.; Xu, J.-T.; Du, B.-Y.; Fan, Z.-Q.; Wang, X. Inorganic-Salt-Induced Morphological Transformation of Semicrystalline Micelles of PCL-B-PEO Block Copolymer in Aqueous Solution. *Macromolecular Chemistry and Physics* **2010**, *211* (17), 1909–1916.

[24] He, W.-N.; Zhou, B.; Xu, J.-T.; Du, B.-Y.; Fan, Z.-Q. Two Growth Modes of Semicrystalline Cylindrical Poly(ε-Caprolactone)-B-Poly(ethylene Oxide) Micelles. *Macromolecules* **2012**, *45* (24), 9768–9778.

[25] Du, Z.-X.; Xu, J.T.; Fan, Z.Q. Regulation of Micellar Morphology of PCL-B-PEO Block Copolymers by Crystallization Temperature. *Macromol. Rapid Commun.* **2008**, *29* (6), 467–471.

[26] Yang, J.X.; He, W.N; Xu, J.X.; Du, B.Y.; Fan, Z.Q. Influence of Different Inorganic Salts on Crystallization-Driven Morphological Transformation of PCL-B-PEO Micelles in Aqueous Solutions. *Chin J Polym Sci* **2014**, *32* (9), 1128–1138.

[27] Schmelz, J.; Schedl, A. E.; Steinlein, C.; Manners, I.; Schmalz, H. Length Control and Block-Type Architectures in Worm-like Micelles with Polyethylene Cores. *J. Am. Chem. Soc.* **2012**, *134* (34), 14217–14225.

[28] Schmalz, H.; Schmelz, J.; Drechsler, M.; Yuan, J.; Walther, A.; Schweimer, K.; Mihut, A. M. Thermo-Reversible Formation of Wormlike Micelles with a Microphase-Separated Corona from a Semicrystalline Triblock Terpolymer. *Macromolecules* **2008**, *41* (9), 3235–3242.

[29] Fan, B.; Liu, L.; Li, J.-H.; Ke, X.-X.; Xu, J.-T.; Du, B.-Y.; Fan, Z.-Q. Crystallization-Driven One-Dimensional Self-Assembly of Polyethylene-B-Poly(tert-Butylacrylate) Diblock

Copolymers in DMF: Effects of Crystallization Temperature and the Corona-Forming Block. *Soft Matter* **2015**, *12* (1), 67–76

[30] Gilroy, J. B.; Lunn, D. J.; Patra, S. K.; Whittell, G. R.; Winnik, M. A.; Manners, I. Fiber-like Micelles via the Crystallization-Driven Solution Self-Assembly of Poly(3-Hexylthiophene)-Block-Poly(methyl Methacrylate) Copolymers. *Macromolecules* **2012**, *45* (14), 5806–5815.

[31] Qian, J.; Li, X.; Lunn, D. J.; Gwyther, J.; Hudson, Z. M.; Kynaston, E.; Rupar, P. A.; Winnik, M. A.; Manners, I. Uniform, High Aspect Ratio Fiber-like Micelles and Block Co-Micelles with a Crystalline π-Conjugated Polythiophene Core by Self-Seeding. *J. Am. Chem. Soc.* **2014**, *136* (11), 4121–4124.

[32] Kynaston, E. L.; Gould, O. E. C.; Gwyther, J.; Whittell, G. R.; Winnik, M. A.; Manners, I. Fiber-Like Micelles from the Crystallization-Driven Self-Assembly of Poly(3-Heptylselenophene)-Block-Polystyrene. *Macromol. Chem. Phys.* **2015**, *216* (6), 685–695.

[33] Petzetakis, N.; Dove, A. P.; O'Reilly, R. K. Cylindrical Micelles from the Living Crystallization-Driven Self-Assembly of Poly(lactide)-Containing Block Copolymers. *Chem. Sci.* **2011**, *2* (5), 955.

[34] Petzetakis, N.; Walker, D.; Dove, A. P.; O'Reilly, R. K. Crystallization-Driven Sphere-to-Rod Transition of Poly(lactide)-B-Poly(acrylic Acid) Diblock Copolymers: Mechanism and Kinetics. *Soft Matter* **2012**, *8* (28), 7408–7414.

[35] Sun, L.; Petzetakis, N.; Pitto-Barry, A.; Schiller, T. L.; Kirby, N.; Keddie, D. J.; Boyd, B. J.; O'Reilly, R. K.; Dove, A. P. Tuning the Size of Cylindrical Micelles from Poly(l-Lactide)-B-Poly(acrylic Acid) Diblock Copolymers Based on Crystallization-Driven Self-Assembly. *Macromolecules* **2013**, *46* (22), 9074–9082.

[36] Qian, J.; Guerin, G.; Lu, Y.; Cambridge, G.; Manners, I.; Winnik, M. A. Self-Seeding in One Dimension: An Approach To Control the Length of Fiberlike Polyisoprene–Polyferrocenylsilane Block Copolymer Micelles. *Angew. Chem. Int. Ed. Engl.* **2011**, *50*, 1622–1625.

[37] Qian, J.; Lu, Y.; Cambridge, G.; Guerin, G.; Manners, I.; Winnik, M. A. Polyferrocenylsilane Crystals in Nanoconfinement: Fragmentation, Dissolution, and Regrowth of Cylindrical

Block Copolymer Micelles with a Crystalline Core. *Macromolecules* **2012**, *45* (20), 8363–8372.

[38] Qian, J.; Lu, Y.; Chia, A.; Zhang, M.; Rupar, P. A.; Gunari, N.; Walker, G. C.; Cambridge, G.; He, F.; Guerin, G.; et al. Self-Seeding in One Dimension: A Route to Uniform Fiber-like Nanostructures from Block Copolymers with a Crystallizable Core-Forming Block. *ACS Nano* **2013**, *7* (5), 3754–3766.

[39] Qian, J.; Guerin, G.; Cambridge, G.; Manners, I.; Winnik, M. Seeded Growth and Solvent-Induced Fragmentation of Fiber like Polyferrocenylsilane Polyisoprene Block Copolymer Micelles. *Macromol. Rapid Comm.* **2010**, *31* (9–10), 928–933.

[40] Hayward, D. W.; Gilroy, J. B.; Rupar, P. A.; Chabanne, L.; Pizzey, C.; Winnik, M. A.; Whittell, G. R.; Manners, I.; Richardson, R. M. Liquid Crystalline Phase Behavior of Well-Defined Cylindrical Block Copolymer Micelles Using Synchrotron Small-Angle X-Ray Scattering. *Macromolecules* **2015**, *48* (5), 1579–1591.

[41] Guérin, G.; Raez, J.; Manners, I.; Winnik, M. A. Light Scattering Study of Rigid, Rodlike Organometallic Block Copolymer Micelles in Dilute Solution. *Macromolecules* **2005**, *38*, 7819–7827.

[42] Uemura, T.; Kaseda, T.; Sasaki, Y.; Inukai, M.; Toriyama, T.; Takahara, A.; Jinnai, H.; Kitagawa, S. Mixing of Immiscible Polymers Using Nanoporous Coordination Templates. *Nat Commun* **2015**, *6*, 7473.

[43] Jinnai, H.; Spontak, R. J.; Nishi, T. Transmission Electron Microtomography and Polymer Nanostructures. *Macromolecules* **2010**, *43* (4), 1675–1688.

[44] Kawase, N.; Kato, M.; Nishioka, H.; Jinnai, H. Transmission Electron Microtomography without the "missing Wedge" for Quantitative Structural Analysis. *Ultramicroscopy* **2007**, *107* (1), 8–15.

[45] a) Guerin, G.; Qi, F.; Cambridge, G.; Manners, I.; Winnik, M. A. Evaluation of the Cross Section of Elongated Micelles by Static and Dynamic Light Scattering. *J. Phys. Chem. B* **2012**, *116*, 4328–4337. b) Guerin, G.; Qi, F.; Cambridge, G.; Manners, I.; Winnik, M. A. Correction to "Evaluation of the Cross Section of Elongated Micelles by Static and Dynamic Light Scattering."*J. Phys. Chem. B* **2012**, *116*, 7603–7603.

[46] Pedersen, J. S. Analysis of Small-Angle Scattering Data from Colloids and Polymer Solutions: Modeling and Least-Squares Fitting. *Advances in Colloid and Interface Science* **1997**, *70*, 171–210.

[47] Guerin, G.; Wang, H.; Manners, I.; Winnik, M. A. Fragmentation of Fiberlike Structures: Sonication Studies of Cylindrical Block Copolymer Micelles and Behavioral Comparisons to Biological Fibrils. *J. Am. Chem. Soc.* **2008**, *130* (44), 14763–14771.

[48] Sanchez, I. C.; DiMarzio, E. A. Dilute Solution Theory of Polymer Crystal Growth: A Kinetic Theory of Chain Folding. *The Journal of Chemical Physics* **1971**, *55* (2), 893–908.

[49] Gilroy, J. B.; Rupar, P. A.; Whittell, G. R.; Chabanne, L.; Terrill, N. J.; Winnik, M. A.; Manners, I.; Richardson, R. M. Probing the Structure of the Crystalline Core of Field-Aligned, Monodisperse, Cylindrical Polyisoprene-Block-Polyferrocenylsilane Micelles in Solution Using Synchrotron Small- and Wide-Angle X-Ray Scattering. *J. Am. Chem. Soc.* **2011**, *133* (42), 17056–17062.

[50] Vilgis, T.; Halperin, A. Aggregation of Coil-Crystalline Block Copolymers: Equilibrium Crystallization. *Macromolecules* **1991**, *24* (8), 2090–2095.

[51] Cambridge, G.; Gonzalez-Alvarez, M. J.; Guerin, G.; Manners, I.; Winnik, M. A. Solution Self-Assembly of Blends of Crystalline-Coil Polyferrocenylsilane-Block-Polyisoprene with Crystallizable Polyferrocenylsilane Homopolymer. *Macromolecules* **2015**, *48* (3), 707–716.

[52] Shu, R.; Zha, L.; Eman, A. A.; Hu, W. Fibril Crystal Growth in Diblock Copolymer Solutions Studied by Dynamic Monte Carlo Simulations. *J. Phys. Chem. B* **2015**, *119* (18), 5926–5932.

[53] Ungar, G.; Putra, E. G. R.; Silva, D. S. M. de; Shcherbina, M. A.; Waddon, A. J. The Effect of Self-Poisoning on Crystal Morphology and Growth Rates. In *Interphases and Mesophases in Polymer Crystallization I*; Allegra, P. G., Ed.; Advances in Polymer Science; Springer Berlin Heidelberg, 2005; pp 45–87.

[54] Chen, W. Y.; Zheng, J. X.; Cheng, S. Z. D.; Li, C. Y.; Huang, P.; Zhu, L.; Xiong, H.; Ge, Q.; Guo, Y.; Quirk, R. P.; et al. Onset of Tethered Chain Overcrowding. *Phys. Rev. Lett.* **2004**, *93* (2), 28301.

[55] Zheng, J. X.; Xiong, H.; Chen, W. Y.; Lee, K.; Van Horn, R. M.; Quirk, R. P.; Lotz, B.; Thomas, E. L.; Shi, A.-C.; Cheng, S. Z. D. Onsets of Tethered Chain Overcrowding and

Highly Stretched Brush Regime via Crystalline−Amorphous Diblock Copolymers. *Macromolecules* **2006**, *39* (2), 641–650.

[56] Papkov, V. S.; Gerasimov, M. V.; Dubovik, I. I.; Sharma, S.; Dementiev, V. V.; Pannell, K. H. Crystalline Structure of Some Poly(ferrocenylenedialkylsilylenes). *Macromolecules* **2000**, *33* (19), 7107–7115.

[57] Lammertink, R. G. H.; Hempenius, M. A.; Thomas, E. L.; Vancso, G. J. Periodic Organic–organometallic Microdomain Structures in Poly(styrene-Block-Ferrocenyldimethylsilane) Copolymers and Blends with Corresponding Homopolymers. *J. Polym. Sci. B Polym. Phys.* **1999**, *37* (10), 1009–1021.

[58] Rulkens, R.; Lough, A. J.; Manners, I.; Lovelace, S. R.; Grant, C.; Geiger, W. E. Linear Oligo(ferrocenyldimethylsilanes) with between Two and Nine Ferrocene Units: Electrochemical and Structural Models for Poly(ferrocenylsilane) High Polymers. *J. Am. Chem. Soc.* **1996**, *118* (50), 12683–12695.

[59] Lammertink, R. G. H.; Hempenius, M. A.; Vancso, G. J. Crystallization Kinetics and Morphology of Poly(ferrocenyldimethylsilane). *Macromol. Chem. Phys.* **1998**, *199* (10), 2141–2145.